Spontaneous Knotting and Unknotting of Flexible Linear Polymers: Equilibrium and Kinetic Aspects

4 **AUTHORS**, INCLUDING:

Luca Tubiana
Jožef Stefan Institute
15 PUBLICATIONS **168** CITATIONS

Spontaneous Knotting and Unknotting of Flexible Linear Polymers: Equilibrium and Kinetic Aspects

L. Tubiana,[†] A. Rosa,[‡] F. Fragiacomo,[§] and C. Micheletti*[,‡]

[†]Department of Theoretical Physics, Jožef Stefan Institute, SI-1000 Ljubljana, Slovenia
[‡]SISSA—Scuola Internazionale Superiore di Studi Avanzati, Via Bonomea 265, 34136 Trieste, Italy
[§]Dipartimento di Fisica, Università degli Studi di Milano, Via Celoria 16, 20133 Milano, Italy

ABSTRACT: We report on a computational study of the statics and dynamics of long flexible linear polymers that spontaneously knot and unknot. Specifically, the equilibrium self-entanglement properties, such as the knotting probability, knot length and position, are investigated with extensive Monte Carlo sampling of chains of up to 15 000 beads. Tens of such equilibrated chains of up to ∼4000 beads are next used as starting points for Langevin dynamics simulations. The complex interplay of chain dynamics and self-knotting is addressed by monitoring the time evolution of various metric and entanglement properties. In particular, the extensive duration of the simulations allows for observing the spontaneous formation and disappearance of prime and composite physical knots in linear chains. Notably, a sizable fraction of self-knotting and unknotting events is found to involve regions that are far away from the chain termini. To the best of our knowledge, this represents the first instance where spontaneous changes in knotting for linear homopolymers are systematically characterized using unbiased dynamics simulations.
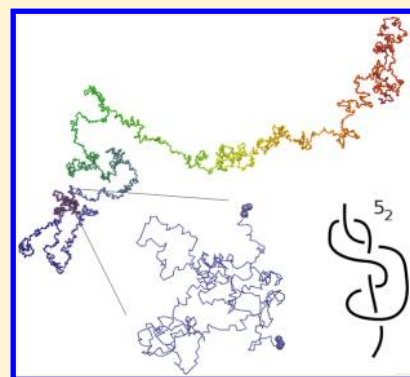
1. INTRODUCTION

Polymer entanglement has been long studied for its impact on the statics and dynamics of dense systems, of which artificial polymer melts and tightly packed biofilaments represent two notable instances. One particular form of entanglement is given by knots, which are ubiquitous in long flexible chains[1] and are known to affect their physical and functional properties.[2−11]

These aspects have so far been mainly studied for chains that form rings by circularization. In such case, in fact, the topological state of the chain can be rigorously defined and can be analyzed with established mathematical procedures.[7,12−14]

In contrast to the case of circular chains, proper mathematical knots can not be defined in linear chains with free ends. Yet, we know by experience that localized, "physical" knots do appear in sufficiently long open chains and can be long-lived. Indeed, the relatively unexplored topic of physical knots is gaining increasing attention because of its relevance in nanotechnological contexts, especially regarding the implications for polymers mechanical resistance, rheology and pore translocation capabilities. In fact, recent related studies have addressed the problem of how a designed tightly knotted linear chain disentangles,[15−18] how it responds to stretching,[19−25] and how knotted proteins[26] and knotted nucleic acids[27] translocate through a solid-state nanopore.

Arguably, the simplest system where the influence of knotting on the properties of linear polymers can be investigated is represented by long flexible linear chains in equilibrium. Such reference system has recently been studied to establish the equilibrium knotting probability[28] and knot size of

flexible chains of beads consisting of up to 1000 monomers.[29] However, to the best of our knowledge, no study has yet focused on the kinetics of knotting and unknotting in such system, nor in other homopolymeric systems.

Here, building on these previous studies, we extend the characterization of the entanglement of unconstrained linear chains in two directions. Specifically, we push the statics profiling to linear chains composed of up to 15000 beads and, especially, we address the role of chain dynamics in the knotting of flexible homopolymers.

2. METHODS

The statics and dynamics of fully flexible self-avoiding chains of beads were characterized with stochastic numerical techniques. For computational efficiency, Monte Carlo (MC) simulations were used for the equilibrium properties, while kinetic ones were addressed with a Langevin molecular dynamics (MD) scheme. The two simulation techniques were applied to different, but physically equivalent, models of flexible self-avoiding chains, as detailed below.

2.1. Equilibrium: Monte Carlo Simulations. The equilibrium properties were computed for self-avoiding freely jointed chains consisting of up to $N = 15000$ spherical beads. The beads diameter, σ, is taken as the unit of length.

Starting from a straight chain configuration, the conformational space was explored using a standard MC scheme employing unrestricted crankshaft and pivot moves.[13] A trial configuration generated by either type of move was rejected if it violated self-

avoidance due to the presence of overlapping beads, and accepted otherwise. All self-avoiding configurations were therefore sampled with the same statistical weight. A sample configuration of $N = 8192$ beads is shown in Figure 1.
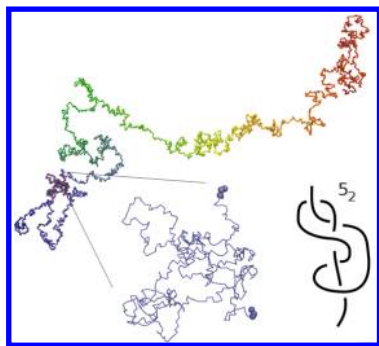

Figure 1. Typical configuration of a knotted chain composed by $N = 8192$ beads sampled with the Monte Carlo scheme. The chain backbone is colored with a rainbow scheme along the contour. The expanded region is the knotted portion of the chain, which corresponds to a 5_2 knot. A simplified, schematic diagram of the 5_2 knot is shown at the bottom on the right. For clarity, the chain backbone in the expanded view is shown with a thin line. To represent the chain excluded volume, a few chain beads of the expanded region are explicitly represented.

For each chain length, we gathered $\sim 10^5 - 10^6$ uncorrelated configurations generated by the MC procedure, and used them to calculate the expectation values of various observables, such as the fraction of knotted chains, the incidence of various knot types and their contour length; see section 2.3.

2.2. Kinetics: Molecular Dynamics Simulations. Because of the fixed-bond length constraint, the freely jointed chain model is not well-suited for efficient MD simulations. To this purpose we therefore resorted to the flexible chain-of-beads model of Kremer and Grest.[30]

In the following, the position in space of the center of the ith bead is indicated with $\vec{r}_i$ while the distance vector of beads i and j is denoted as $\vec{d}_{i,j} = \vec{r}_j - \vec{r}_i$ and its norm simply as $d_{i,j}$. The model Hamiltonian is

$$\mathcal{H} = \sum_{i=1}^{N-1} \left[U_{\text{FENE}}(i, i+1) + \sum_{j=i+1}^{N} U_{\text{LJ}}(i, j) \right] \tag{1}$$

where i and j run over the beads indices, U_{LJ} enforces the excluded volume interaction between distinct beads (including consecutive ones), and U_{FENE} enforces chain connectivity. The complete expressions for the two terms are:

$$U_{\text{FENE}}(i, i+1) = \begin{cases} -\dfrac{k}{2} R_0^2 \ln\left[1 - \left(\dfrac{d_{i,i+1}}{R_0}\right)^2 \right], & d_{i,i+1} \le R_0 \\ 0, & d_{i,i+1} > R_0 \end{cases} \tag{2}$$

$$U_{\text{LJ}}(i, j) = \begin{cases} 4\varepsilon\left[\left(\dfrac{\sigma}{d_{i,j}}\right)^{12} - \left(\dfrac{\sigma}{d_{i,j}}\right)^6 + \dfrac{1}{4} \right], & d_{i,j} \le \sigma 2^{1/6} \\ 0, & d_{i,j} > \sigma 2^{1/6} \end{cases} \tag{3}$$

where σ is the nominal bead diameter (which is the unit length), $R_0 = 1.5\sigma$, $k = 30.0\varepsilon/\sigma^2$, and $\varepsilon = 1.0 k_B T$, where $k_B T$ is the equilibrium thermal energy.[30] No hydrodynamic treatment is considered in the model.

The kinetics of chains of length N up to 4096 beads was studied using fixed-volume and constant-temperature MD simulations with implicit solvent. The dynamics was integrated with the LAMMPS

engine[31] with Langevin thermostat. Periodic boundary conditions were applied, with the simulation box chosen large enough in order to avoid chain self-interactions across the boundaries. The elementary integration time step was $\Delta t = 0.012 \tau_{MD}$, where $\tau_{MD} = \sigma(m/\varepsilon)^{1/2}$ is the Lennard-Jones time, m is the bead mass (set equal to the LAMMPS default value), and the friction coefficient, γ, corresponds to $\gamma/m = 0.5 \tau_{MD}^{-1}$.[30]

2.3. Observables. *Autocorrelation Time.* For an overall characterization of the kinetics of the flexible, self-avoiding chains, we considered the time autocorrelation function, $\phi(t)$, of the end-to-end distance vector, $\vec{R}_{ee} = \vec{r}_N - \vec{r}_1$:

$$\phi(t) = \frac{\langle \vec{R}_{ee}(t) \cdot \vec{R}_{ee}(0) \rangle}{\langle \vec{R}_{ee}^2 \rangle} \tag{4}$$

where $\langle \rangle$ denotes the average over simulation time for 10 independent extensive trajectories. According to Rouse theory,[32] the decay of $\phi(t)$ should be described by a sum of exponentials with the slowest effective Rouse decay time, τ_R scaling as $N^{1+2\nu}$. For chains that do not experience self-avoidance the metric exponent ν is equal to 0.5, and hence $\tau_R \propto N^2$, while for self-avoiding chains $\nu \simeq 0.6$ and hence $\tau_R \propto N^{2.2}$.

To calculate the effective decay time of $\phi(t)$ in our MD simulations, we first captured the expected theoretical behavior by fitting it with a sum of two exponentials, $f(t) = a_0 e^{-t/\tau_1} + (1 - a_0)e^{-t/\tau_2}$, and then obtained τ_R by integrating the fitting function, $\tau_R = \int_0^\infty f(t)\, dt = a_0 \tau_1 + (1 - a_0)\tau_2$.

Physical Knots in Linear Chains. The degree of entanglement of equilibrated chains was characterized by computing the chain knotting probability, that is the percentage of MC sampled chains that are knotted. To compute this and other observables it is necessary to suitably extend the standard notion of knottedness. The latter is, in fact, rigorously defined only for chains that are closed (or with suitably constrained termini) as their topological state cannot be altered by continuous, nonsingular chain deformations respecting chain connectivity.

Linear chains can be assigned to a definite, or dominant, knotted topology by bridging the two termini with an auxiliary arc, so to obtain a closed chain for which the topological state is mathematically well-defined. Several such closing procedure were previously introduced.[28,29,33,34] Here we adopted the "minimally-interfering" closure scheme that was recently introduced by some of us.[34] In this method, which is numerically efficient, the auxiliary arc is constructed so to minimize the potential interference due to spurious entanglement of the auxiliary arc with the rest of the linear chain.

After closure into a ring, the chain topology was established by first simplifying the ring geometry with topology-preserving moves,[13,35,36] and finally computing the Alexander determinants $\Delta(t)$ in $t = -1$ and $t = -2$.

Knot Position and Length. The equilibrium and kinetic properties of linear chains with nontrivial topology were further characterized by establishing both the size and position of the knot(s) accommodated along their contour. Specifically, we adopted the bottom-up knot search strategy,[34,37] which consists of locating the shortest chain portion that, upon closure, has the same topology as the whole chain. For a robust result, we required that the knotted portion is strictly smaller than the whole chain and also required that the arc formed by rest of the linear chain plus its minimally interfering closure has (again upon closure) the unknotted topology.

To minimize the computational cost of locating knots, the systematic search of the shortest knotted arc was carried out by moving along the chain contour in steps sizes of up to $N/100$. Here, the size of each step is given by the number of bonds which can be rectified without affecting the topology, according to the simplification scheme described in ref 34.

We expect the results to be largely independent of the specific knot search strategy because the amount of chain entanglement found *a posteriori* in our equilibrated open chains is limited (knotting probability not exceeding 3% for the longest chains). In this situation, in fact, different knot localization methods[28,29,37−39] usually yield
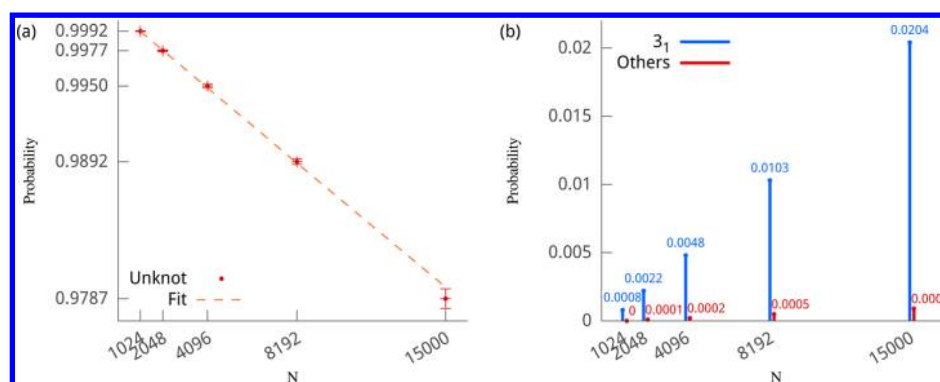
Figure 2. (a) The equilibrium fraction of unknotted chains, P_{UN}, is shown as a function of chain contour length, N. The solid line is the exponential best-fit, Ae^{-N/N_0} which yields $N_0 = (7.1 \pm 0.2) \times 10^5$. (b) Probability of occurrence of trefoil and other knot types versus chain length.

consistent results (this may not hold for strong self-entanglement, see ref 40).

3. RESULTS AND DISCUSSION

3.1. Equilibrium. The MC scheme described in section 2.1 was used to generate equilibrated conformations of self-

Figure 3. (a) Average knot length, $\langle l_k \rangle$, versus chain contour length, N. The solid curve is the best-fit with the function $\langle l_k \rangle = a + b\,N^\alpha$, with $\alpha = 0.44 \pm 0.08$. (b) Probability distribution of l_k for various chain contour lengths. The distributions have an apparent linear trend in a log−log plot (see inset), which is suggestive of a power-law decay. The best linear fit of the log−log data for $l_k > 1500$ and $N > 1024$ yields the power law exponent, -1.5 ± 0.1. The associated power law is illustrated by the slope of the black guideline.

avoiding freely jointed chains of $N = 1024$, 2048, 4096, 8192, and 15000 beads. At each chain length we sampled $10^5 - 10^6$ uncorrelated conformations, which sufficed to gather $\sim 700-2000$ independent knotted chains.

The increase of chain self-entanglement with contour length is illustrated in Figure 2a which reports the fraction of equilibrated configurations that are unknotted. This unknotting probability, P_{UN}, is expected to decay exponentially with N:[1,35,41−44]

$$P_{UN} \simeq e^{-N/N_0} \tag{5}$$

The exponential fit of the data, shown by the dashed curve in Figure 2a, yields $N_0 = (7.1 \pm 0.2) \times 10^5$. This value is in good agreement with the knotting probability previously reported by Virnau et al.[29] for flexible linear chains of up to 1000 beads (for this length it was found $P_{UN} \sim 99.91\%$, similarly to what found here). Furthermore, values with the same order of magnitude, $N_0 \sim 8 \times 10^5$, $N_0 \sim 2.1 \times 10^5$ and $N_0 \sim 1.3 \times 10^5$ were reported respectively for closed self-avoiding chains of beads (as a limiting case of a rod-bead model),[35,43] for rings on the simple cubic lattice[45,46] and rings on the face-centered cubic lattice.[42]

The length-dependent increase of the chain knotting probability is further associated with the appearance of knots of increasing complexity. This fact, which is analogous to the case of closed chains,[7,35,45] is illustrated in Figure 2b. It is seen that the increasing incidence of the simplest knot type, the 3_1 or trefoil knot, is paralleled by the growth of more complex knot types. In particular, at the two largest considered lengths, $N = 8096$ and $N = 15000$ all knots of up to six crossings, with the exception of 6_1, are observed. In particular, we recorded the occurrence of $3_1 \# 3_1$ composite knots, although their quantitative incidence is minimal, ca. 20 instances out of the few thousands sampled knots.

The sizable number of sampled configurations allows for computing the expectation values and the probability distributions of various observables, including some that were not considered in previous investigations of knotted linear chains. A notable one is represented by the average contour length of the knotted region, $\langle l_k \rangle$, which can have important physical reverberations, e.g., on the mechanical resistance of a chain[2,3] or its capability to translocate through pores or openings.[26,27]

The dependence of $\langle l_k \rangle$ on the chain length, N, is shown in the plot of Figure 3a. It should be noted that, because trefoils are by far the dominant knot type for the considered range of N, the ensemble average $\langle l_k \rangle$ essentially reflects the average length of 3_1 knots.

For closed self-avoiding chains it was previously shown that the average length of trefoil knots (and other prime knots, too) follows a power law, $\langle l_k \rangle \propto N^\alpha$.[38,40,47,48] Across these studies, different values of α were reported but all of them were strictly smaller than 1, which indicates a sublinear growth of the average knot length with the chain contour length (weak knot localization[19,28,29])
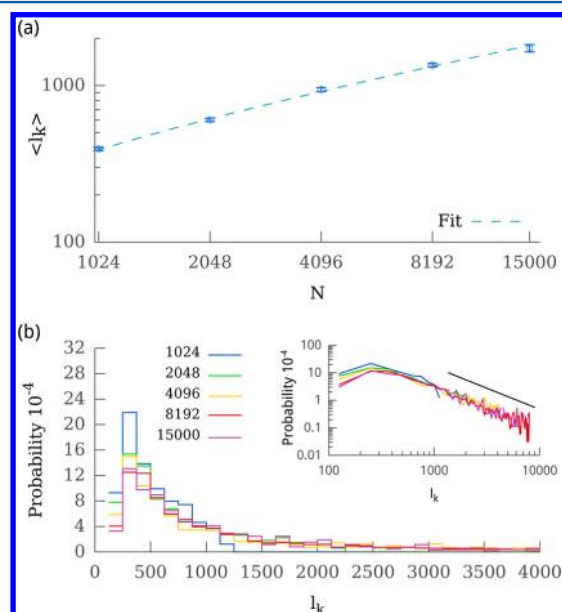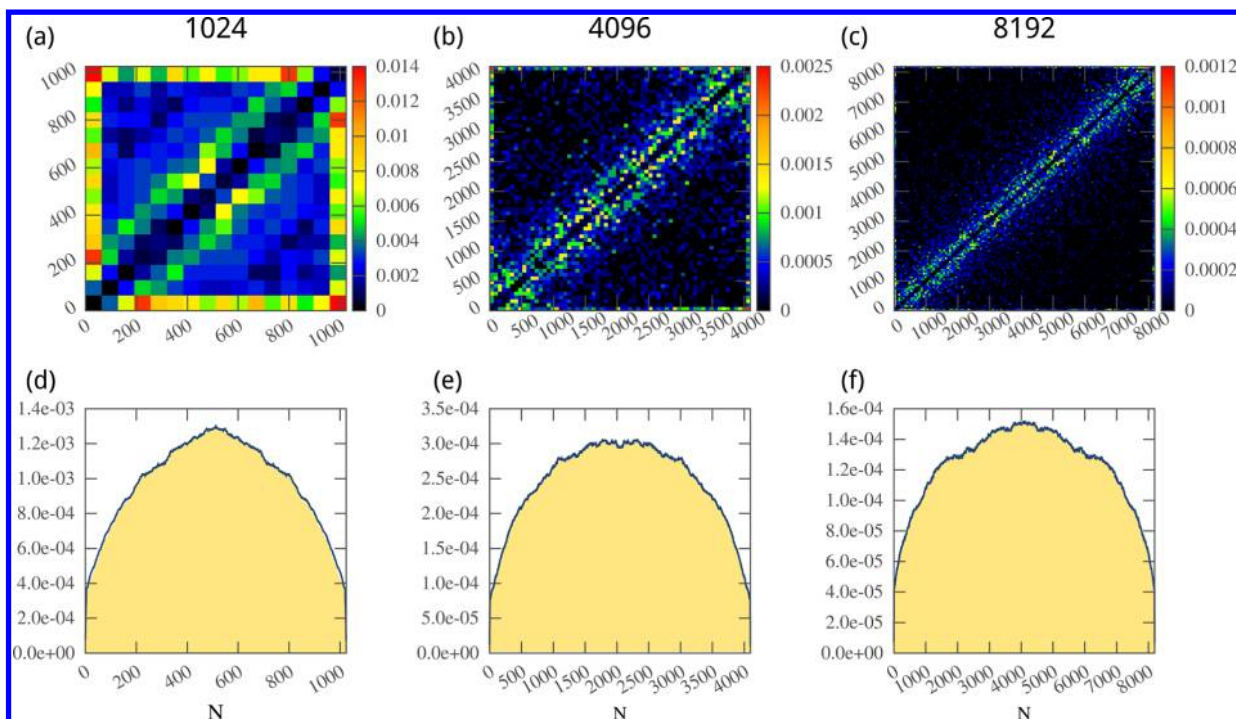
Figure 4. Equilibrium distribution of knots along chains of $N = 1024$, 4096, and 8192 beads. After discretising the knotted chains in segments of 64 beads we computed the (symmetrized) probability, $p(i,j)$ that two given segments, i and j accommodate the ends of a knot. The resulting $p(i,j)$ matrices are shown as color-coded maps in the top row panels a−c. We next calculated the probability that any given chain bead falls within a knotted region. The resulting probability profiles for various chain lengths are shown in panels d, e, and f. The chain-reversal symmetry was used to improve the statistics of all the plots.
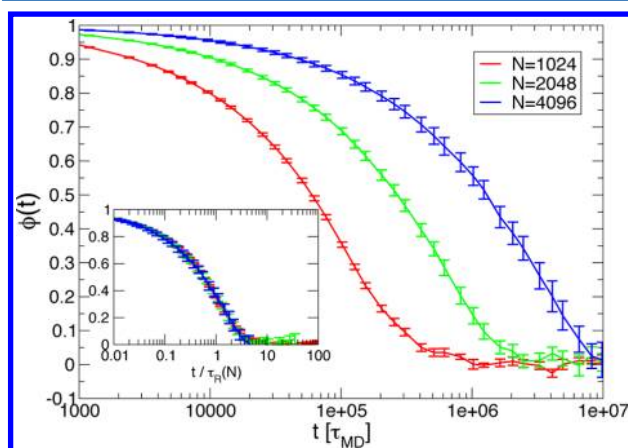

Figure 5. Time autocorrelation function, $\phi(t)$ of the end-to-end distance vector. The data points are obtained by averaging over 10 independent Langevin dynamics trajectories. The bars indicate the standard error of the mean. Inset: the good superposition of the rescaled autocorrelation functions, $\phi(t/\tau_R(N))$ confirms that the decay of $\phi(t)$ is controlled by one dominant time scale compatible with theoretical Rouse time, τ_R.

We observe that unconstrained linear chains display the same weak localization property. In fact, the data for $\langle l_k \rangle$ are well-interpolated by a power law with exponent $\alpha = 0.44 \pm 0.08$, see Figure 3a. This exponent is compatible with the one estimated by Farago et al.[19] for mechanically stretched chains $\alpha = 0.4$, though it differs from the one reported for linear chains of up to $N = 1000$ beads, $\alpha = 0.65$.[29] We note that the gap with this previously reported value can be bridged by considering only the data for $N \leq 4096$, which yields $\alpha \sim 0.6$. This observation points out that current estimates of α may still be affected by

appreciable finite size effects due to the fact that the accessible range of N is still significantly smaller than N_0.

Valuable insight into the dependence of $\langle l_k \rangle$ on N emerges by examining the probability distribution of l_k, which is shown in Figure 3b. First, it is seen that the location of the peaks of the distributions show a very weak, if any, dependence on N. As a matter of fact, they all fall in the 100−300 range. Second, the probability distributions extend appreciably beyond the peak value with a decay compatible with a power-law, see inset in Figure 3b.

Accordingly, knots with length exceeding by several times the most probable (modal) value of $\langle l_k \rangle$ can occur with non-negligible probability. These findings, which parallel the behavior of knotted chains subject to spatial confinement (see Figure 4e in ref 49), indicate that the observed increase of $\langle l_k \rangle$ with N, results from the lack of a definite upper cutoff length of the distribution support. As a result, longer chains can accommodate a sizable population of knots with length that increasingly deviates from the most probable one. A similar effect was previously suggested for closed rings in ref 48.

As a next step for characterizing the relationship between knot length and chain length, we computed the probability that the two ends of the knotted region fall in specific points of the chain. The results are shown in the density plot of Figure 4. It is seen that the probability distribution is fairly uniform in the chain interior. Apart from a localized enhancement very close to the two termini (possibly due to effect of the auxiliary closing arc), the probability density drops near the chain ends. The width of this depletion region at the chain edges is largely independent of N, and about equal to 200. The latter value about coincides with the typical modal value of l_k, suggesting that the depletion arises because of the impossibility to fully
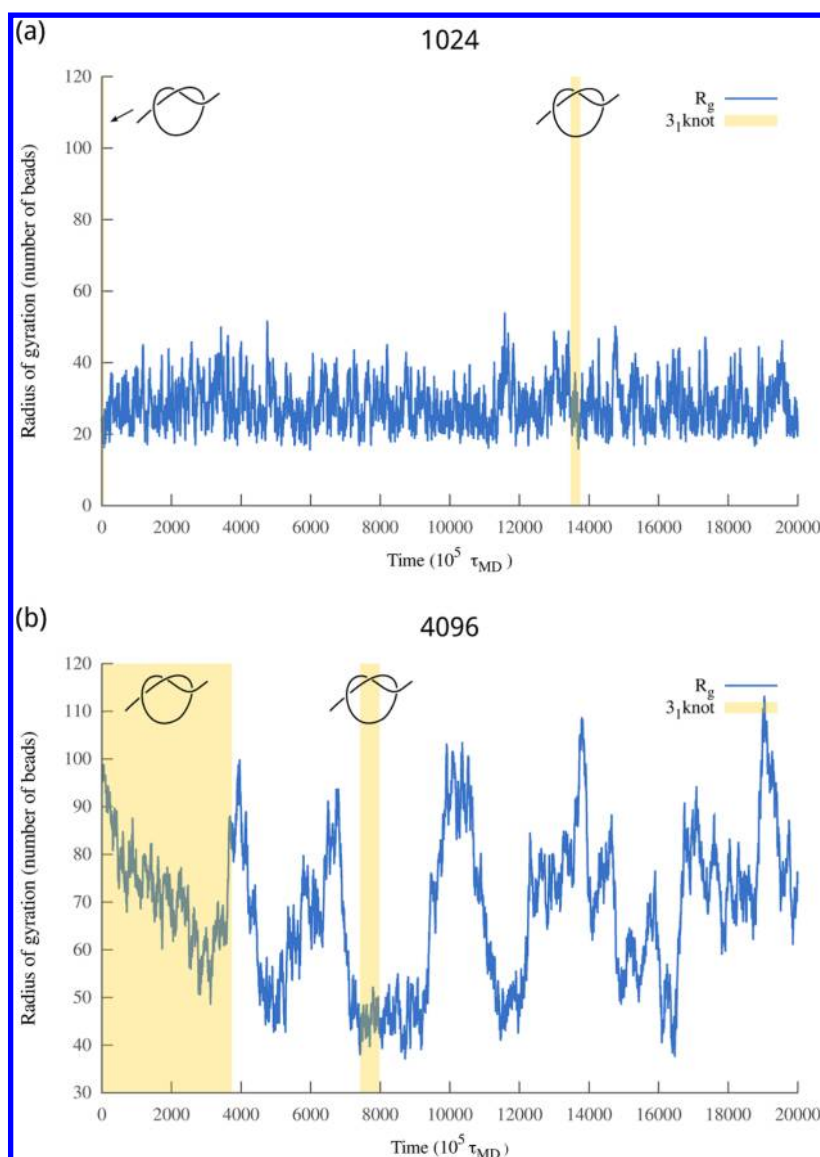
Figure 6. Typical evolution of the metric and topological properties of two initially knotted chains of (a) $N = 1024$ and (b) $N = 4096$ beads. In both cases, the initial configuration accommodated a trefoil knot at the chain center. The metric properties are captured by the chain radius of gyration (blue curve) while the time intervals where the chain is knotted are shown with a colored background. Spontaneous unknotting and knotting events are clearly visible. In both cases, the spontaneously formed knots have the dominant, 3_1 topology.

accommodate knots with the most probable length near the chain ends.

To further characterize the relation between chain length and knot length we computed the probability that any given chain bead falls within a knotted region. The probability profiles, which were calculated considering only knotted chains, are shown in Figure 4d−f for chains of length $N = 1024$, 4096, and 8192, respectively. The appearance of the distributions is center-symmetric and unimodal and the central region acquires a flatter character for increasing N. The properties of the profiles are consistent with the above-mentioned depletion effect near the chain edges.

3.2. Dynamics. Following previous studies of knotted closed chains,[5,50−52] we start the dynamics analysis by comparing the characteristic time scales over which metric and topological properties evolve. Next, we address how the knotting properties observed in equilibrium are linked to the

kinetics of spontaneous formation or untying of knots and their change in size and position along the chain contour.

The characterization of these kinetic properties is based on Langevin dynamics simulations for flexible, self-avoiding chains of $N = 1024$, 2048, and 4096 beads. As described in the Methods, the chain model employed in the Langevin simulations is physically equivalent, but not identical to the one used in Monte Carlo simulations. In particular, the constraints of fixed bond length and sharp excluded volume interactions are softened to be amenable to numerical dynamics simulations.

To optimally monitor the temporal persistence of knots and their motion along the chain contour, we used a specific subset of MC-generated chains as starting configurations. Specifically, we focused on chains which, in their center, accommodate a trefoil knot with length l_k in the 100−300 range. The trefoil topology was picked because it is the dominant one at the considered chain lengths, while the length range was chosen
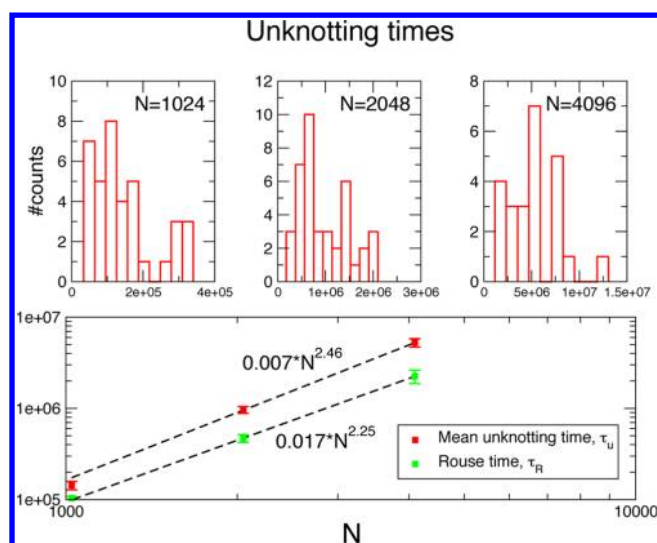
Figure 7. (Top) Distribution of unknotting times for chains of N = 1024, 2048, and 4096 beads. (Bottom) Scatter plots of the mean unknotting (red symbols) and Rouse (green symbols) times versus N. The dashed curves are the power-law best fits. Times are given in units of τ_{MD}.

because it straddles the most probable knot length for all values of N, see Figure 3. For each chain length, we considered about 30 different initial conformations.

3.3. Metric and Topological Autocorrelation Times. As a term of reference we first computed the characteristic time scale for chain metric properties. To do so, we calculated the

end-to-end distance autocorrelation function, $\phi(t)$, over extensive MD simulations, see Figure 5. The characteristic decay time of $\phi(t)$, the so-called Rouse time, τ_R is about $1.04 \times 10^5 \, \tau_{MD}$, $\simeq 4.7 \times 10^5 \tau_{MD}$, and $\simeq 2.25 \times 10^6 \tau_{MD}$ for N = 1024, 2048, and 4096, respectively. Bearing in mind the limitations of the small set of considered chain lengths, the power-law best fit gives $\tau_R \propto N^{2.25}$, in good accord with theoretical arguments;[32] see Methods.

The typical evolution of chain topology over time scales much longer than τ_R is illustrated in Figure 6, which also indicates with a colored overlay, whether knots are present or absent during the dynamical evolution.

In both examples, it is seen that after the untying of the initial knot the chain remains mostly unknotted for the rest of the simulation, with the exception of transient self-knotting events. The sparse occurrence of knots is consistent with the low incidence of knots observed in equilibrium (which should coincide with the time-averaged knotting probability in asymptotically long dynamical trajectories); see, e.g., Figure 2.

The distribution of times required to spontaneously untie the trefoil knot initially centered in the middle of the chain, is shown in the top panels of Figure 7 for various values of N. It is seen that the broad range of unknotting times covered by the distributions grows noticeably with N. Indeed, the average unknotting time, τ_u takes on the values $\simeq 1.43 \times 10^5 \tau_{MD}$, $\simeq 9.67 \times 10^5 \tau_{MD}$, $\simeq 52.5 \times 10^5 \tau_{MD}$, for N = 1024, 2048, and 4096, respectively. As shown in the bottom panel of Figure 7, these values are not only larger than the corresponding Rouse times, but their scaling, $\propto N^{2.46}$, is also characterized by a larger exponent than τ_R.
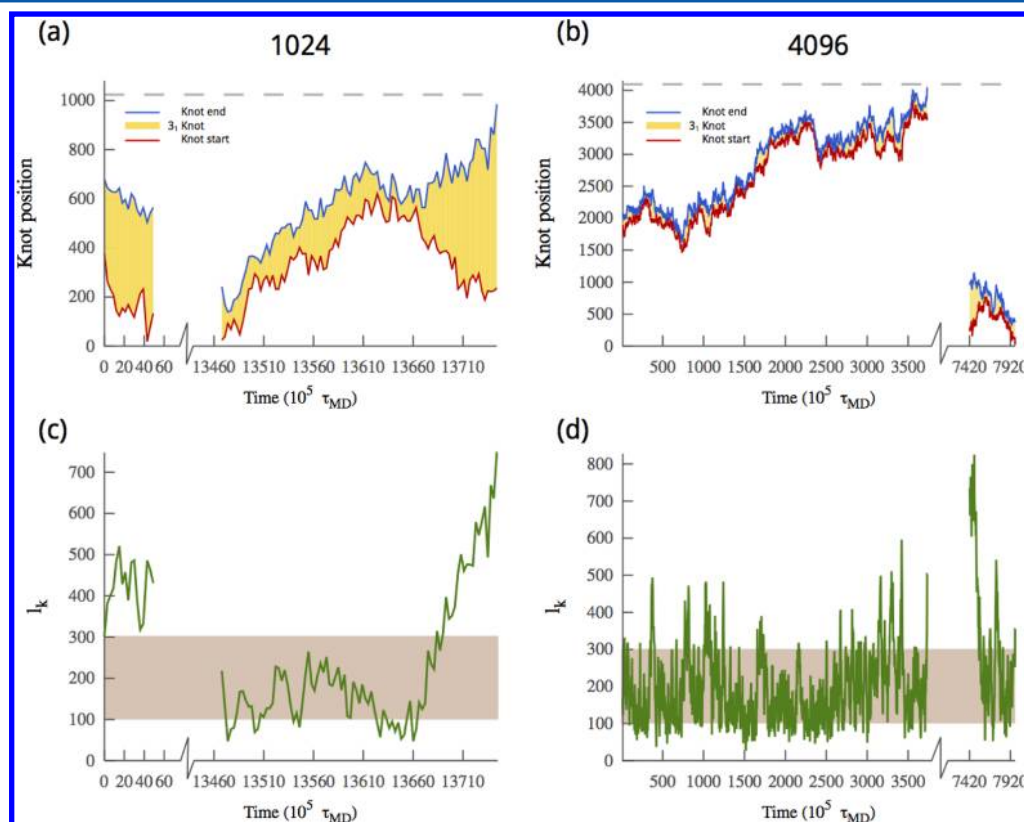

Figure 8. Detailed characterization of the knotting kinetics for the two trajectories shown in Figure 6. The upper panels illustrate the time-evolution, along the chain contour, of the two ends of the knot, marked in red and blue. The knotted region is highlighted in yellow. The evolution of the knot contour length, l_k, is shown in the bottom panels (c and d). The brown overlay highlights the most probable range of l_k, see Figure 3.
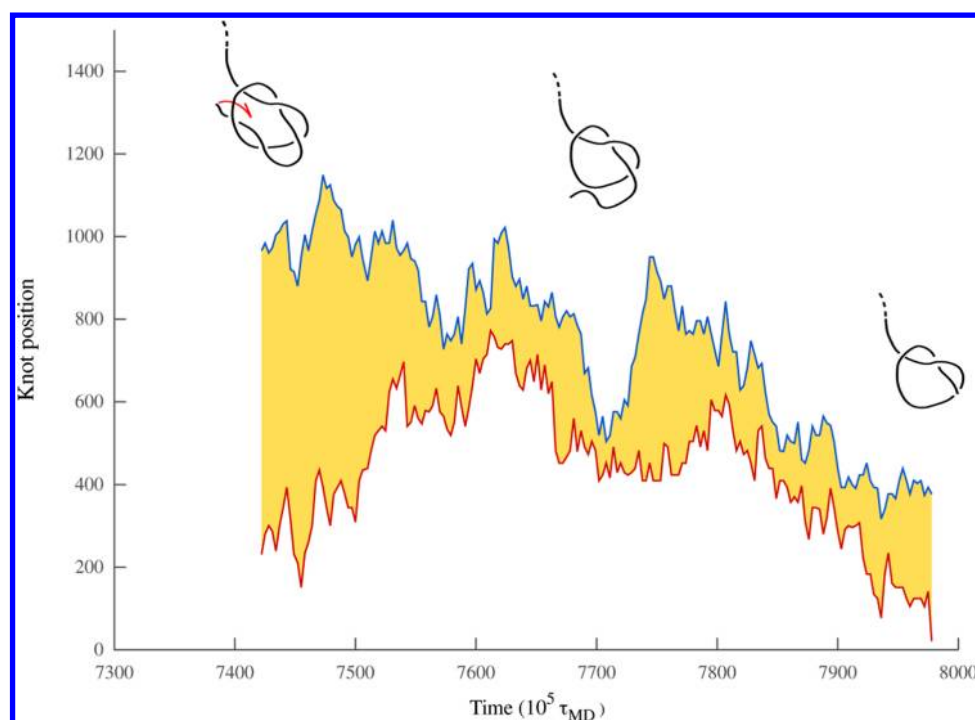
Figure 9. Detailed characterization of the spontaneous knotting event shown in Figures 6b and 8b for a chain of $N = 4096$ beads. The knot suddenly appears at a finite distance (ca. 200 beads) from the nearest chain end. The mechanism of knot formation is shown schematically in the upper plot and involves a slipknot stage. Notice that the resulting trefoil is atypically large as it covers about one-third of the chain contour.

Although the uncertainty on the effective scaling exponent is sizable, 15%, due to the limited set of considered chain lengths, the visual inspection of the trends of τ_R and τ_u in Figure 7 supports the faster increase of τ_u over τ_R. Indeed, τ_u/τ_R ranges from $\simeq 1.4$ for $N = 1024$ to 2.3 for $N = 4096$.

Because this different growth is suggestive of a nontrivial interplay of changes in chain geometry and the modes of chain unknotting, we believe it would be most interesting to further address this specific point in future studies by considering much longer chains. Further motivations for such extensions are provided in the next sections in connection with the mechanism presiding the spontaneous formation or untying of knots and their motion along the chain contour.

3.4. Spontaneous Knotting and Unknotting Events. To elucidate the mechanisms leading to spontaneous knotting and unknotting events, we have monitored the knots position and length during the simulations.

Figure 8 presents these quantities for the two trajectories previously illustrated in Figure 6. It is seen that the knot moves away from its initial central location with a stochastic motion along the chain contour. The motion of the two knot ends, though not exactly concerted, is visibly correlated. In fact, as illustrated in panels c and d of Figure 8, the knot length, l_k, mostly fluctuates in the range covered by the peak of the equilibrium l_k distribution, see Figure 3.

By examining the traces in parts a and b of Figure 8, one observes that the first unknotting event occurs when one of the two knot ends reaches one of the chain termini. Analogous considerations can be made for the other changes of topology illustrated in the two panels. We emphasize that this is the first time that spontaneous knotting events are systematically observed in unbiased MD simulations of a general homopolymer model.

Notice, in particular, that for the illustrated $N = 1024$ case, a trefoil knot is formed at one end, travels to the center of the chain where it swells along the chain contour and finally unties by slipping off the other chain end. The lifespan of this knot, which crosses the whole chain, is larger than the time required for the initial knot (positioned in the chain center) to untie. Throughout the collected simulations, such long-lived knots are uncommon. In fact, the typical "life-cycle" of a knot is akin to the one shown for the longer chain, $N = 4096$, in panel (b). As it can be seen, the knot which is formed spontaneously at one end, briefly diffuses toward the chain interior before slipping out of the same end from where it originated.

While most of the knots spontaneously form or untie at the chain ends, a small, but sizable, fraction of knotting/unknotting events occur via a mechanism that, borrowing the terminology introduced in protein-related contexts,[53,54] can be termed as slipknotting.

These knotting events occur when a hairpin-bent portion of the chain enters a preformed loop and drags the entire terminal segment through it (while the time-reversed procedure leads to unknotting). The mechanism, which was recently reported and discussed in folding simulations of knotted proteins[54] is sketched in Figure 9. This figure also illustrates the time-evolution of the two ends of a trefoil knot that forms via slipknotting and dissolves by slipping out of the chain. Notice that, at variance with the more intuitive case of knots forming or disappearing at the chain ends, slipknotting events do not necessarily occur near the chain termini. As illustrated in Figure 9, they, in fact, generally manifest by the sudden appearance of a knotted region far away from the termini.

The relevant question that emerges from the results discussed above regards the relative incidence of the two types of knotting/unknotting events, namely those occurring at the chain termini or via slipknotting. To this purpose, we
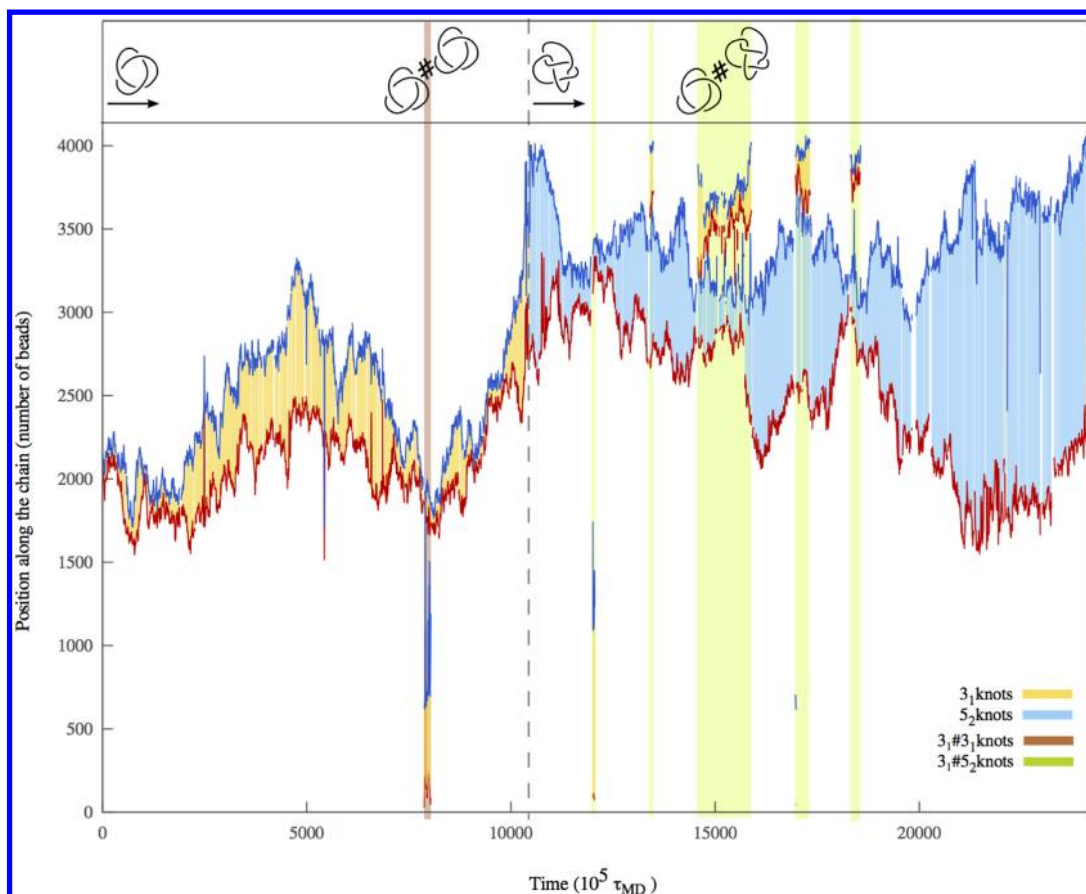
Figure 10. Dynamical evolution of a chain of $N = 4096$ beads exhibiting several transitions of knots topologies. In particular, one observes both changes in knot topology ($3_1 \rightarrow 5_2$) as well as the formation of composite knots. In the latter case, the separate prime components are well identifiable as shown by the colored overlays. The various encountered knotted topologies are illustrated at the top with schematic conventional knot diagrams. Notice that the conventional "ring" diagrams are used while the considered chain is actually linear.

gathered 90 extensive trajectories throughout the considered range of N and counted how many of their 134 spontaneous events of knot formation/disappearance occurred at a distance of at least 100 beads from the chain termini. This threshold length was chosen because it exceeds by ten times the typical contour distance traveled by the knot ends in two consecutive snapshots of the recorded trajectories. The criterion therefore provides a conservative counting of the number of slipknotting events. It is found that 11 of the topology changes, corresponding to ~10% of all knotting or unknotting events, involve slipknotting.

This clarifies that slipknotting though not representing the dominant knotting mode for the considered flexible linear chains still accounts for a sizable fraction of their spontaneous topology changes.

Furthermore, because the two mechanisms differ for their local/nonlocal character it may be envisaged that their relative incidence could be significantly affected by the length of the chain. As a matter of fact, none of the observed slipknotting events took place in the shortest chains, $N = 1024$, but occurred exclusively for $N = 2048$ and $N = 4096$. This provides a further element of interest to address in future investigations of knotted chains. In particular, one may anticipate that the balance of the two mechanisms could have important reverberations regarding the dependence of the unknotting time on N, too.

3.5. Formation of Composite Knots. We conclude the analysis of the system dynamics by discussing notable, though rare, instances where chain topology changes by the incremental addition (and subsequent removal) of entanglement to an already-knotted chain.

The trajectory shown in Figure 10 provides a remarkable illustration of this point. In fact, one first observes that the initial 3_1 knot evolves transiently into a $3_1\#3_1$ composite knot due to the temporary formation of an additional trefoil knot at one of the termini. At a later time, after reverting to the 3_1 topology, the knot becomes a 5_2 knot. Next, a further trefoil-knotting event occurs through slipknotting and the chain acquires a $5_2\#3_1$ topology. Finally, after an intermittent formation/disruption of the slipknotted trefoil (arguably due to a persistent chain geometry) the chain goes back to the 5_2 topology, then the 3_1 one and finally it unties itself.

One aspect that is highlighted in Figure 10 is that the composite knots $3_1\#3_1$ and $3_1\#5_2$ present well separated prime components. This fact is consistent with the observed dynamics of knot formation: because knots tend to originate at chain ends and their length grows sublinearly with chain contour length, one can expect that composite knots can form by incremental addition of individual prime components. Aside from these kinetic mechanisms, we note that across the limited number of composite knots sampled with the equilibrium MC simulations, no appreciable overlap was found for the individual prime components.

4. SUMMARY AND CONCLUSIONS

We have presented a numerical study of the spontaneous occurrence of knots in free long flexible chains of beads. The study was carried out at two levels. First we addressed the equilibrium entanglement, that is the knotting probability, knot size and location along the chain, by Monte Carlo sampling of chains with up to $N = 15000$ beads. This represents a more than 10-fold extension in length over previous studies of entanglement in flexible linear chains. Second, by using extensive Langevin dynamics on chains with up to $N = 4096$ beads, we provide the first investigation of the connection between the equilibrium entanglement properties and the free polymer dynamics.

For the equilibrium properties we find that characteristic length controlling the N-dependent exponential decrease of unknotted chains is $N_0 \sim 7.1 \times 10^5$ beads (implying a 2% knotting probability for the longest chains, $N = 15000$). The knotting probability profile is depleted near the ends of the chain over a region of width of about 200 beads. This boundary effect appears related to the most probable size of knots, which falls in the 100–300 beads range independent of the chain contour length. However, because the knot length probability distribution decays slowly the average knot size does increase with N, albeit sublinearly (weak knot localization).

Regarding the dynamical properties, over an extensive set of simulated trajectories, we observed the occurrence of more than 100 spontaneous knotting and unknotting events. These changes in topology typically involve the chain ends, when a loop is threaded (or unthreaded) by one of the chain termini. However, about 10% of the knotting or unknotting events are shown to form via a different mechanism which causes knots to tie or untie away from the chain termini.

Because of the relative weight, these two mechanisms could depend on the chain contour lengths, we think that it would be most interesting to address this point in future studies by extending the chain length. By doing so it also ought to be possible to characterize the impact of these mechanisms on the knot mean lifetime and its relationship with the chain global relaxation time.

■ AUTHOR INFORMATION

Corresponding Author
*E-mail: (C.M.) michelet@sissa.it.

Notes
The authors declare no competing financial interest.

■ REFERENCES

(1) Sumners, D. W.; Whittington, S. G. *J. Phys. A: Math. Gen.* **1988**, 21, 1689.
(2) Saitta, A. M.; Soper, P. D.; Wasserman, E.; Klein, M. L. *Nature* **1999**, 399, 46–48.
(3) Arai, Y.; Yasuda, R.; Akashi, K.; Harada, Y.; Miyata, H.; Kinosita, K.; Itoh, H. *Nature* **1999**, 399, 446–448.
(4) Katritch, V.; Bednar, J.; Michoud, D.; Scharein, R. G.; Dubochet, J.; Stasiak, A. *Nature* **1996**, 384, 142–145.
(5) Orlandini, E.; Stella, A. L.; Vanderzande, C.; Zonta, F. *J. Phys. A: Math. Theor.* **2008**, 41, 122002.
(6) Crisona, N. J.; Weinberg, R. L.; Peter, B. J.; Sumners, D. W.; Cozzarelli, N. R. *J. Mol. Biol.* **1999**, 289, 747–775.
(7) Orlandini, E.; Whittington, S. G. *Rev. Mod. Phys.* **2007**, 79, 611–642.
(8) Marenduzzo, D.; Micheletti, C.; Orlandini, E. *J. Phys. Condens. Mat.* **2010**, 22, 283102–283102.
(9) Kanaeda, N.; Deguchi, T. *Phys. Rev. E* **2009**, 79, 021806.
(10) Grosberg, A. Y.; Rabin, Y. *Phys. Rev. Lett.* **2007**, 99, 217801.
(11) Rosa, A.; Orlandini, E.; Tubiana, L.; Micheletti, C. *Macromolecules* **2011**, 44, 8668–8680.
(12) Meluzzi, D.; Smith, D. E.; Arya, G. *Annu. Rev. Biophys.* **2010**, 39, 349–366.
(13) Micheletti, C.; Marenduzzo, D.; Orlandini, E. *Phys. Rep.* **2011**, 504, 1–73.
(14) Grosberg, A. Y. *Polym. Sci. Ser. A* **2009**, 51, 70.
(15) Kim, E.-G.; Klein, M. L. *Macromolecules* **2004**, 37, 1674–1677.
(16) Möbius, W.; Frey, E.; Gerland, U. *Nano Lett.* **2008**, 8, 4518–4522.
(17) Ben-Naim, E.; Daya, Z. A.; Vorobieff, P.; Ecke, R. E. *Phys. Rev. Lett.* **2001**, 86, 1414–1417.
(18) Metzler, R.; Reisner, W.; Riehn, R.; Austin, R.; Tegenfeldt, J. O.; Sokolov, I. M. *Europhys. Lett.* **2006**, 76, 696.
(19) Farago, O.; Kantor, Y.; Kardar, M. *Europhys. Lett.* **2002**, 60, 53–59.
(20) Bao, X. R.; Lee, H. J.; Quake, S. R. *Phys. Rev. Lett.* **2003**, 91, 265506.
(21) Huang, L.; Makarov, D. E. *J. Phys. Chem. A* **2007**, 111, 10338–10344.
(22) Zheng, X.; Vologodskii, A. *Phys. Rev. E* **2010**, 81, 041806.
(23) Kirmizialtin, S.; Makarov, D. E. *J. Chem. Phys.* **2008**, 128, 094901–094901.
(24) Matthews, R.; Louis, A. A.; Yeomans, J. M. *EPL (Europhys. Lett.)* **2010**, 89, 20001.
(25) Matthews, R.; Louis, A. A.; Likos, C. N. *ACS Macro Lett.* **2012**, 1, 1352–1356.
(26) Huang, L.; Makarov, D. E. *J. Chem. Phys.* **2008**, 129, 121107.
(27) Rosa, A.; Di Ventra, M.; Micheletti, C. *Phys. Rev. Lett.* **2012**, 109, 118301.
(28) Millett, K.; Dobay, A.; Stasiak, A. *Macromolecules* **2005**, 38, 601.
(29) Virnau, P.; Kantor, Y.; Kardar, M. *J. Am. Chem. Soc.* **2005**, 127, 15102–15106.
(30) Kremer, K.; Grest, G. S. *J. Chem. Phys.* **1990**, 92, 5057.
(31) Plimpton, S. J. *J. Comput. Phys.* **1995**, 117, 1–19.
(32) Doi, M.; Edwards, S. F. *The Theory of Polymer Dynamics*; Oxford University Press: New York, 1986.
(33) Janse van Rensburg, E. J.; Sumners, D. A. W.; Wasserman, E.; Whittington, S. G. *J. Phys. A: Math. Gen.* **1992**, 25, 6557.
(34) Tubiana, L.; Orlandini, E.; Micheletti, C. *Prog. Theor. Phys. Supp.* **2011**, 191, 192–204.
(35) Koniaris, K.; Muthukumar, M. *Phys. Rev. Lett.* **1991**, 66, 2211–2214.
(36) Taylor, W. R. *Nature* **2000**, 406, 916–919.
(37) Katritch, V.; Olson, W. K.; Vologodskii, A.; Dubochet, J.; Stasiak, A. *Phys. Rev. E* **2000**, 61, 5545–5549.
(38) Marcone, B.; Orlandini, E.; Stella, A. L.; Zonta, F. *Phys. Rev. E* **2007**, 75, 041105.
(39) Mansfield, M. L. *Macromolecules* **1998**, 31, 4030–4032.
(40) Tubiana, L.; Orlandini, E.; Micheletti, C. *Phys. Rev. Lett.* **2011**, 107, 188302.
(41) Michels, J. P. J.; Wiegel, F. W. **1986**, 403, 269–284.
(42) Janse van Rensburg, E. J.; Whittington, S. G. *J. Phys. A: Math. Gen.* **1990**, 23, 3573.
(43) Koniaris, K.; Muthukumar, M. *J. Chem. Phys.* **1991**, 95, 2873–2881.
(44) Shimamura, M. K.; Deguchi, T. *Phys. Lett. A* **2000**, 274, 184–191.
(45) Janse van Rensburg, E. J. *Contemp. Math.* **2002**, 304, 125–136.
(46) Baiesi, M.; Orlandini, E.; Stella, A. L. *J. Stat. Mech.: Theory E* **2010**, 2010, P06012.

(47) Orlandini, E.; Tesi, M. C.; Janse van Rensburg, E. J.; Whittington, S. G. *J. Phys. A: Math. Gen.* **1998**, *31*, 5953.

(48) Mansfield, M. L.; Douglas, J. F. *J. Chem. Phys.* **2010**, *133*, 044903.

(49) Micheletti, C.; Orlandini, E. *Soft Matter* **2012**, *8*, 10959−10968.

(50) Quake, S. R. *Phys. Rev. Lett.* **1994**, *73*, 3317.

(51) Sheng, Y. J.; Lai, P. Y.; Tsao, H. K. *Phys. Rev. E* **1998**, *58*, 1222−1225.

(52) Mansfield, M. L.; Douglas, J. F. *J. Chem. Phys.* **2010**, *133*, 044904.

(53) King, N. P.; Yeates, E. O.; Yeates, T. O. *J. Mol. Biol.* **2007**, *373*, 153−166.

(54) Sułkowska, J. I.; Sułkowski, P.; Onuchic, J. *Proc. Natl. Acad. Sci. U.S.A.* **2009**, *106*, 3119−3124.